Directing Energy Transport in Organic Photovoltaic Cells Using Interfacial Exciton Gates

S. Matthew Menke,[†] Tyler K. Mullenbach,[†] and Russell J. Holmes*

Department of Chemical Engineering and Materials Science University of Minnesota 421 Washington Avenue Southeast, 151 Amundson Hall, Minneapolis, Minnesota 55455, United States. [†]Equal contribution to this work.

ABSTRACT Exciton transport in organic semiconductors is a critical, mediating process in many optoelectronic devices. Often, the diffusive and subdiffusive nature of excitons in these systems can limit device performance, motivating the development of strategies to direct exciton transport. In this work, directed exciton transport is achieved with the incorporation of exciton permeable interfaces. These interfaces introduce a symmetry-breaking imbalance in exciton energy transfer, leading to directed motion. Despite their obvious utility for enhanced exciton harvesting in organic photovoltaic cells (OPVs), the emergent properties of these interfaces are as yet uncharacterized. Here, directed exciton transport is conclusively demonstrated in both dilute donor and energy-cascade OPVs where judicious optimization of the interface allows exciton transport to the donor–acceptor heterojunction to occur considerably faster than when relying on simple diffusion. Generalized systems incorporating multiple exciton permeable interfaces are also explored, demonstrating the ability to further harness this phenomenon and expeditiously direct exciton motion, overcoming the diffusive limit.

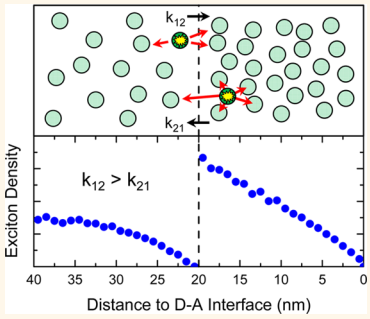

KEYWORDS: exciton · transport · energy transfer · diffusion · organic semiconductor · photovoltaic cell · OPV

Photovoltaic cells based on organic semiconductors are attractive for their inherent compatibility with lightweight substrates and high throughput processing techniques.[1] Indeed, the performance of these devices continues to increase, with multiple groups reporting devices having efficiencies in the range of 8–12%.[2–8] To realize efficient power conversion, the tightly bound excitons generated under optical excitation must be efficiently dissociated, and the constituent electronic charges separated and collected.[9] The excitonic character of the excited state thus introduces a unique challenge into the photoconversion process, namely, how to realize dissociation and maximize exciton harvesting. In most organic photovoltaic cells (OPVs), dissociation is affected at an electron donor–acceptor (D–A) interface. Consequently, the efficiency of exciton harvesting depends strongly on the ability of excitons to reach the D–A interface. Straightforward exciton migration is often exacerbated by a short exciton diffusion length (L_D), relative to the optical absorption length in most organic semiconductors.[10]

To date, researchers have responded to the discrepancy between L_D and the absorption length in two ways. The first, involves the use of techniques to increase the bulk diffusion length of the organic active materials.[11–20] While some success along these lines has been realized, the observed increases in L_D have not to date translated into record efficiency operation. The second approach is to utilize the bulk heterojunction (BHJ) architecture in which the donor and acceptor materials are blended in order to realize a large interfacial area for dissociation, and continuous pathways for charge collection.[21,22] The BHJ is ubiquitous in the field of OPVs, and altogether circumvents the exciton transport step, presenting instead the new challenge of how best to engineer film morphology to satisfy the simultaneous constraints for efficient exciton and charge harvesting.[23]

Much effort in the optimization of OPV architecture reflects a fundamental challenge in solid-state physics, namely, how to direct the motion of the neutral exciton. In inorganic semiconductors, excitonic phenomena are often not considered at room

* Address correspondence to rholmes@umn.edu.

Received for review February 20, 2015 and accepted March 12, 2015.

Published online March 23, 2015
10.1021/acsnano.5b01160

temperature due to their low binding energy and straightforward dissociation *via* thermal energy.[24] When present, the large radius of the Wannier-Mott-type excitons of these systems permits some degree of spatial manipulation *via* applied electric fields.[25−27] In organic semiconductors, the localized Frenkel-type exciton is strongly bound, making manipulation with an applied field more difficult. In fact, a consistent scheme for biasing exciton motion has yet to be presented in organic semiconductors. The ability to direct exciton transport would have broad application, of particular note for exciton harvesting and photoconversion in an OPV.

Here, we demonstrate the usefulness of a to-date, untapped route for directed energy transfer and enhanced exciton diffusion in organic semiconductors. In particular, we demonstrate that while gains in exciton harvesting are possible with enhanced bulk L_D, a more effective approach involves introducing exciton permeable interfaces that intentionally bias energy transfer toward the D−A interface. Such passive exciton gates break the symmetry associated with normal diffusion and exploit transport in an apparent superdiffusive regime. With the use of these interfaces, large diffusion efficiencies are realized without the need to increase the area of the dissociating interface. Here, the diffusion efficiency (η_D) refers to the probability that a photogenerated exciton within an active layer samples the D−A interface.

A passive exciton gate may be realized at the interface between two materials (Figure 1a) where there exists an imbalance in the forward and reverse exciton transfer rates. This imbalance may arise from a number of different material or device configurations. For example, *Material 1* in Figure 1a may be a donor material with a larger energy gap than *Material 2*.[28,29] A pair of donor layers satisfying this criterion is often a critical component of an energy-cascade OPV.[3,30−34] In such a structure, an exciton to the left of the interface has a nonzero probability of moving either left or right, while an exciton on the right of the interface may only move to the right due to conservation of energy. Thus, an interface of this type relies on an energetic asymmetry to realize the required rate imbalance.

A second configuration that can lead to a similar asymmetry in rates requires an interface between dilute and neat layers of a single active molecular species.[11,34] Using the schematic of Figure 1a, *Material 1* is a layer of donor material diluted into a wide energy gap matrix, while *Material 2* is a neat layer of the same donor. In this configuration, there is no energetic asymmetry as the exciton is confined to the donor species on both sides of the interface. There is, however, a difference in the molecular site density between the dilute and neat materials, creating the required asymmetry. For an exciton immediately to the left of this interface, dilution reduces the number of molecular destination sites in the dilute layer relative to the neat layer, and the same holds for excitons on the right side of the interface. Since the rate of hopping is proportional to the number of sites, the site imbalance creates an asymmetry in hopping rates.

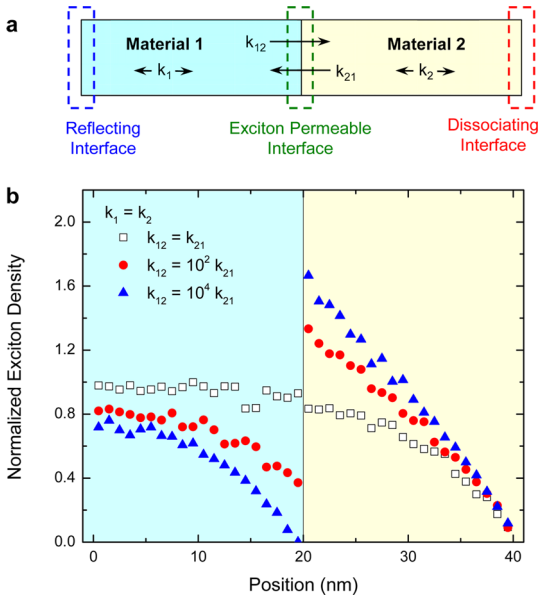

Figure 1. (a) Exciton permeable interfaces are characterized by nondestructive flux between two materials. The imbalance at the interface is defined as k_{12}/k_{21}. (b) Normalized exciton density for the schematic system as a function of imbalance at the permeable interface. Here, the increasing imbalance in energy transfer leads directly to a discontinuity in the exciton density, characterized by the depletion and pile-up of excitons on the side of the interface to which energy transfer is favored.

RESULTS AND DISCUSSION

Here, we present results demonstrating exciton gating and enhanced exciton transport for architectures exploiting both the energetic and site density asymmetries discussed above. To isolate the role of the interface in determining the overall efficiency of exciton transport, a Kinetic Monte Carlo (KMC) formalism is developed to solve the 1-D exciton diffusion equation across exciton permeable interfaces. The advantage of this stochastic solution is that the boundary condition for the permeable interface does not need to be known *a priori*, and can be, instead, constructed by identifying the imbalance in exciton energy transfer rates at the interface. Other device related boundary conditions, such as exciton reflecting and dissociating, may also be easily incorporated as appropriate.[35] Care is taken to ensure that the KMC solutions agree with analytical solutions for cases without permeable interfaces. Figure 1b demonstrates the drastic effect that an imbalance in energy transfer rates can impart on the steady state exciton density in a model OPV multilayer system. Here, k_{12} and k_{21} are the energy transfer rates to *Material 2* and *Material 1*, respectively. When the rates are equal, no imbalance is present and the

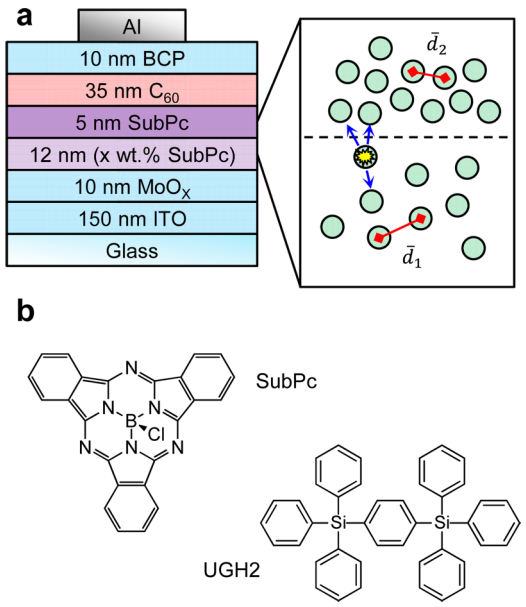

Figure 2. (a) The layer structure for a dilute donor OPV where directed exciton transport results from an imbalance in molecular site density and intermolecular separation ($\bar{d}_1 > \bar{d}_2$). (b) Molecular structures for SubPc and UGH2.

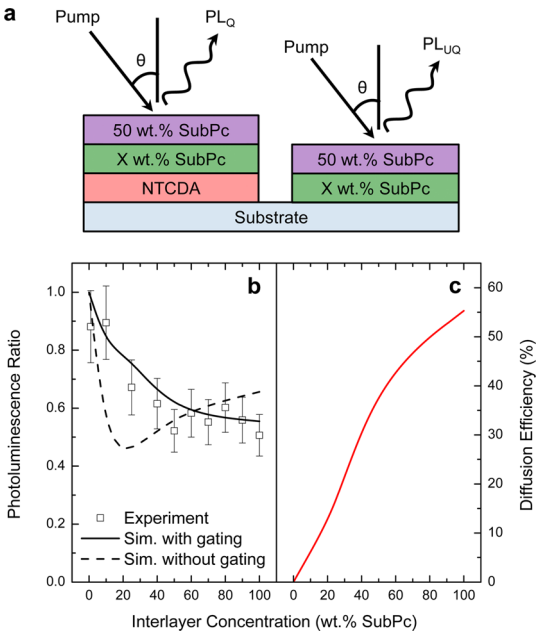

Figure 3. (a) Schematic for the multilayer photoluminescence quenching experiment designed to confirm the presence of exciton gating at the permeable interface located between the 50 wt % and *X* wt % SubPc layers. (b) Experimental and simulated photoluminescence ratios as a function of interlayer concentration. Simulations are shown for results with and without accounting for gating at the exciton permeable interface. (c) Also shown is the tabulated exciton diffusion efficiency as a function of interlayer concentration when gating is properly included.

conventional, continuous solution is retained. The presence of imbalance, however, leads to a discontinuity in the exciton density at the permeable interface. The discontinuity reflects a depletion and pile-up of excitons, with a net movement toward the side of the interface to which energy transfer is favored. In this model system, the imbalance at the interface is beneficial for exciton motion rightwards, thereby also increasing the flux of excitons toward the dissociating interface adjacent to *Material 2*.

As discussed, the interface between dilute and neat layers of donor material forms an exciton gate due to an asymmetry in transfer rates. Recently, such dilute donor OPVs have shown a 30% enhancement in η_P relative to undiluted control devices.[11] In these devices, dilute layers of the archetypical electron donating molecule boron subphthalocyanine chloride[36−38] (SubPc) dispersed in the wider energy-gap host material *p*-bis(triphenylsilyl)benzene[39] (UGH2) show a 50% increase in the L_D of SubPc owing to optimized Förster energy transfer and intermolecular interaction. The increase in bulk L_D leads to an enhancement in η_D when incorporated as part of a multilayer donor structure (Figure 2a). Notably, an exciton permeable interface exists between the 12 nm-thick dilute layer of variable concentration and the 5 nm-thick layer of neat SubPc. Note that the undiluted control device is optimized with a 13 nm-thick layer of SubPc. The enhancement in η_D for these structures is, consequently, a combination of both bulk diffusion and interface effects. To model exciton migration in these devices, proper consideration of energy transfer at the permeable interface is critical. In addition to the imbalance in molecular site density, the variation in average intermolecular separation ($\bar{d}_1 > \bar{d}_2$) manifests imbalance across the permeable interface through the concentration dependence of the self-Förster radius (self-R_0) and the distance dependence for the rate of Förster energy transfer. These contributions are pictured schematically in Figure 2a.

To confirm the validity of this model, photoluminescence quenching experiments and complementary simulations were performed for a two-layer system where the outer layer consists of a 20 nm-thick layer of 50 wt % SubPc dispersed in UGH2, while the 10 nm-thick inner layer has a variable SubPc concentration (Figure 3a). Photoluminescence (PL) is measured with and without the presence of an adjacent 10 nm-thick layer of naphthalene-1,4,5,8-tetracarboxylic acid dianhydride (NTCDA). Experimental photoluminescence ratios are defined as the ratio between quenched photoluminescence (PL_Q) and unquenched photoluminescence (PL_{UQ}). Simulated photoluminescence ratios are generated using the KMC approach for two situations namely, with and without the rate imbalance at the exciton permeable interface. Modeling the experimental photoluminescence ratios, consequently, provides a direct confirmation for the presence and the sources of the rate imbalance. Further experimental details can be found in the Supporting Information.

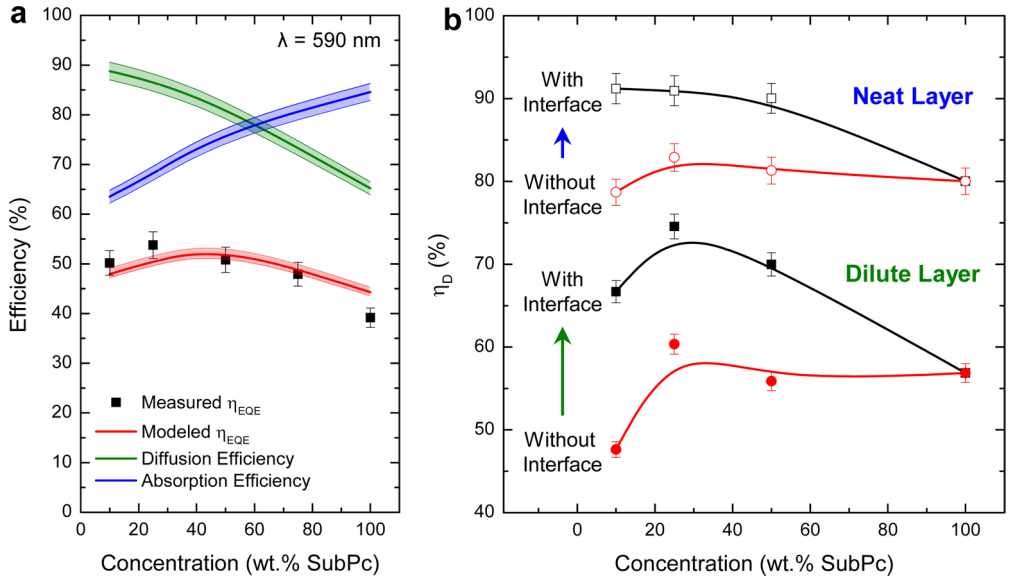

Figure 4. (a) Simulated and measured η_{EQE} for dilute donor OPVs as well as the corresponding absorption (η_A) and diffusion (η_D) efficiencies. (b) Separated η_D for the dilute and neat layers as a function of dilute layer concentration and comparison of an artificial OPV that has no imbalance at the permeable interface. While the artificial devices only account for changes in the bulk L_D with dilution, significant enhancements in the η_D are achieved when the imbalance at the permeable interface is included.

Agreement between experimental and simulated photoluminescence ratios is only achieved when imbalance (gating) at the permeable interface is included (Figure 3b). Interestingly, when the effect of the exciton permeable interface is correctly included, η_D is optimized for an inner layer comprised of undiluted SubPc (Figure 3c). This counterintuitive result contrasts the notion that exciton harvesting is optimized by incorporating active materials with the longest L_D and confirms that the interface plays a critical role in driving excitons toward the D−A interface. This result has not previously been reported or quantified in OPVs and provides an entirely new axis for device design.

Figure 4a shows the measured external quantum efficiency (η_{EQE}) at a wavelength λ = 590 nm, corresponding mainly to SubPc absorption, as measured for the architecture in Figure 2 from ref 7.[11] A transfer matrix formalism is employed to model the incident optical field responsible for photon absorption and exciton generation.[35] Simulated values of the η_{EQE}, absorption efficiency (η_A), and η_D are calculated using the KMC model and are shown as a function of dilute layer concentration. Excellent agreement with experiment is found when an additional, concentration independent loss term equal to 0.85 is included. Here, $\eta_{EQE} = \eta_A\eta_D\eta_{CT}\eta_{CC} = 0.85\eta_A\eta_D$ where η_{CT} and η_{CC} are the charge transfer and charge collection efficiencies, respectively. Losses are expected and may reflect exciton quenching at the MoO_x anode buffer layer and a nonunity collection efficiency.[40] Previous work has shown that the acceptor η_{EQE} and device fill factor remain constant for all dilutions ≥25 wt % SubPc, precluding a concentration-dependent value of η_{CC}.[11] Interestingly, η_D increases continuously upon dilution.

To confirm the origin of the enhanced η_D, Figure 4b displays the separated diffusion efficiencies for the dilute (η_D^{Dilute}) and neat layer (η_D^{Neat}) as a function of concentration. The separate values of η_D are simulated for the actual device (Figure 2a) with a rate imbalance at the interface as well as for an artificial device where no imbalance is present. For the latter, the hopping rates within and between each layer are identical, and the exciton lifetimes are adjusted to reflect the proper bulk L_D (see Supporting Information). Here, $L_D = (D\tau)^{1/2}$ where D is the exciton diffusivity, related to the rate of energy transfer, and τ is the exciton lifetime. The simulation of the artificial devices allows for the determination of η_D based solely on changes to the bulk L_D. Dilution is capable of achieving very large imbalances ($k_{12}/k_{21} \sim 100-1000$) in energy transfer, yielding η_D^{Dilute} and η_D^{Neat} significantly larger than those obtained from simply considering increases in bulk L_D. The η_D^{Neat} increases upon dilution owing to more effective reflection at the gating interface due to a reduction in k_{21}. The η_D^{Dilute} increases from η_D^{Dilute} = (56.9 ± 1.1)% to a maximum value of η_D^{Dilute} = (74.6 ± 1.5)%. Of this enhancement, 20% results from favorable changes in bulk L_D with the remainder resulting from the gating effect of the interface. It should be noted that the η_D^{Dilute} increase shown here is compared to a 13 nm-thick neat layer of SubPc. If it was compared to an equally thick layer (17 nm), the increase would be even larger. Remarkably, a total donor layer η_D > 85% is achieved without resorting to a corrugated interface morphology or a BHJ architecture where the large D−A interfacial area circumvents diffusion altogether. This imbalance is also achieved for a flat energetic landscape that, in principle, creates no significant asymmetry for charge transport.

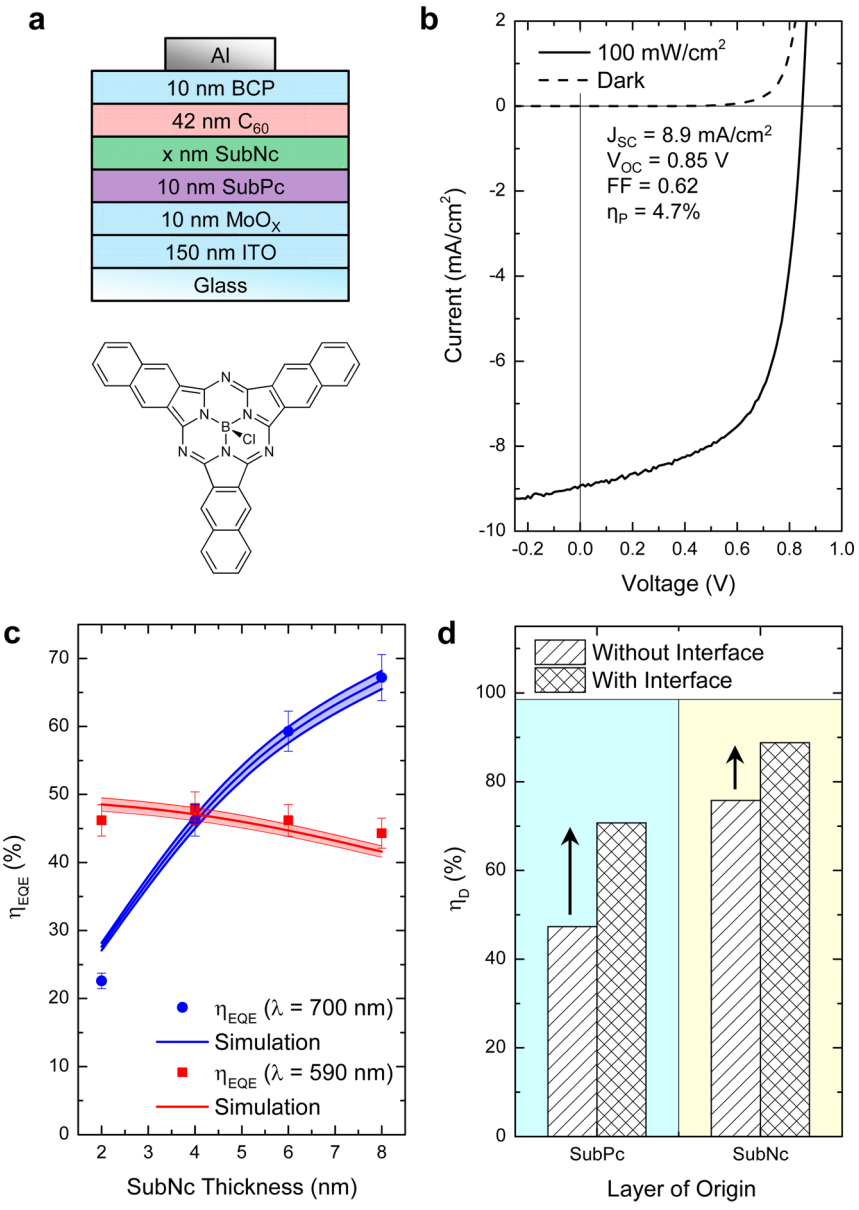

Figure 5. (a) The layer structure for energy-cascade OPVs where exciton energy transfer between wide energy gap SubPc and narrow energy gap SubNc. Also shown is the molecular structure for SubNc. (b) Current–density–voltage characteristics for the champion cell incorporating a 6 nm-thick layer of SubNc measured at 100 mW/cm^2 AM1.5G solar illumination. (c) Simulated and measured η_{EQE} at wavelengths corresponding to regions of predominant absorption for both SubPc and SubNc, respectively. (d) Simulated η_D for both SubPc and SubNc for the as measured OPV as well as an artificial OPV that has no imbalance at the permeable interface.

Beyond dilute donors, examples of other OPV architectures that incorporate passive exciton gates exist—yet remain under-characterized. This stochastic approach, however, can elucidate the exact nature of exciton transport in these devices. Energy-cascade OPVs, for example, derive an imbalance in energy transfer from differences in energy gap. In such a configuration, downhill and sometimes long-range energy transfer[41,42] can take place from a larger energy-gap donor to a lower energy-gap donor as is the case for SubPc (E_g = 2.0 eV) to boron subnaphthalocyanine chloride (SubNc, E_g = 1.8 eV).[43,44] Förster-type energy transfer from SubPc to SubNc is favorable due to their complementary photoluminescence and absorption spectra. A prediction for the Förster radius[45,46] (R_0) from SubPc to SubNc yields R_0 = 2.1 nm, whereas the reverse transfer is very improbable with $R_0 \sim 0$ nm. Therefore, a perfect rate imbalance can be achieved leading to enhanced η_D in both donor layers. In this work, energy-cascade OPVs are fabricated according to the layer structure in Figure 5a where the total donor layer consists of a 10 nm-thick layer of SubPc followed by a variable thickness layer of SubNc. A 42 nm-thick C_{60} acceptor layer is used followed by a 10 nm-thick bathocuproine (BCP) exciton blocking layer and a 100 nm-thick Al cathode. Measurements of

the power conversion efficiency (η_P) reveal that these devices can be quite efficient with η_P = (4.4 ± 0.2)% when incorporating a 6 nm-thick SubNc layer. The current−density−voltage characteristics of the champion cell are shown in Figure 5b. For comparison, the η_P values for single, neat donor planar heterojunction OPVs paired with a C_{60} acceptor based on SubPc and SubNc are η_P = 3.3% and η_P = 2.4%, respectively.

The KMC model for exciton diffusion in cascade structures incorporating exciton permeable interfaces allows for the accurate prediction of the η_{EQE}. Here, the η_{EQE} is modeled for SubPc and SubNc at λ = 590 and 700 nm, respectively, corresponding to regions of predominant absorption for each material, respectively (Figure 5c). The KMC model accurately reproduces the experimentally obtained η_{EQE} with L_D = 15 nm for SubNc and the previously measured value of L_D = 10.7 nm for SubPc.[11] A thickness independent loss term of 0.75 is needed to make the KMC predicted η_{EQE} agree with the measured η_{EQE}. Such a loss term is expected since the KMC model does not address charge collection losses, similar to the dilute devices discussed previously.

To directly investigate the effect of the exciton permeable interface on η_D in this energy-cascade structure, η_D is separately simulated for each donor layer and compared to a device where no imbalance is present at the interface (see Supporting Information). Only excitons generated in SubPc will contribute to the η_D^{SubPc}, with the same being true for excitons generated on SubNc and the η_D^{SubNc}. As can be seen from Figure 5d, the addition of the interface increases the diffusion efficiency for the SubPc and SubNc layers by 50% and 20%, respectively. The increase in the η_D^{SubPc} is a result of directed energy transfer to the SubNc layer at the exciton permeable interface. Since there can be no reverse energy transfer from SubNc to SubPc, excitons that are generated in the SubNc layer experience effective reflection at the permeable interface, thereby also increasing η_D^{SubNc}. Such drastic effects on η_D, and ultimately device photocurrent, can only be quantified by correctly modeling the imbalance in energy transfer at the exciton permeable interface.

So far, only systems incorporating a single permeable interface have been studied, warranting further investigation into multiple interface systems. Inspection of the mean-squared displacement as a function of time elucidates the connection between number of permeable interfaces and the nature of exciton diffusion. To do so, a generic system consisting of 16 1 nm-thick bins is modeled. The first interface is introduced by discretizing the system into two layers, one representing a very dilute layer (*e.g.*, 1 wt %) with L_D = 10 nm and one representing a nearly undiluted layer (*e.g.*, 99 wt %) with L_D = 1 nm, depicted schematically in Figure 6a. Rates are extracted from L_D with a lifetime of τ = 1 ns. A simple molecular site density rationale

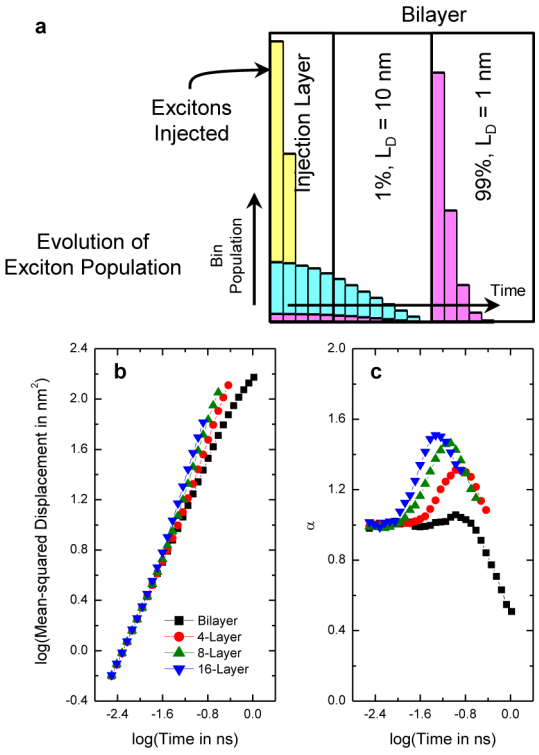

Figure 6. (a) Scheme describing the model experiment where imbalance is derived from differences in molecular concentration. (b and c) Mean-squared displacement and α ($\langle x^2 \rangle = \beta t^{\alpha}$) *versus* time as a function of the number of exciton permeable interfaces. The increase in slope in (b) signals an α > 1, indicating apparent superdiffusive exciton transport.

is used for quantifying the imbalance in energy transfer at the interface(s). To inspect the mean-squared displacement *versus* time, a large population of excitons is injected through a 5 nm-thick layer of the most dilute material and into the multiple interface system. Importantly, the simulation is ended when the first excitons reach the opposite side of the structure. The system is further discretized into 4, 8, and 16 layers containing 3, 7, and 15 exciton permeable interfaces, respectively. A linear interpolation is used to determine the specific rates of energy transfer and relevant molecular concentrations for each layer. For example, the 4-layer system would contain layers with concentrations of 1, 34, 67, and 100 wt % with corresponding L_D of 10, 8.2, 5.8, and 1 nm, respectively.

Figure 6b shows the mean-squared displacement *versus* time for the various multilayer structures. At short times, the structures behave nearly identically. This is consistent since they all contain an identical, 5 nm-thick injection layer whereby the excitons are all sampling an identical, diffusive environment at very short times. However, when the first excitons reach the permeable interface 10−30 ps after injection, the mean-squared displacement begins increasing faster with time, especially for the systems with a larger number of permeable interfaces. In fact, regions of

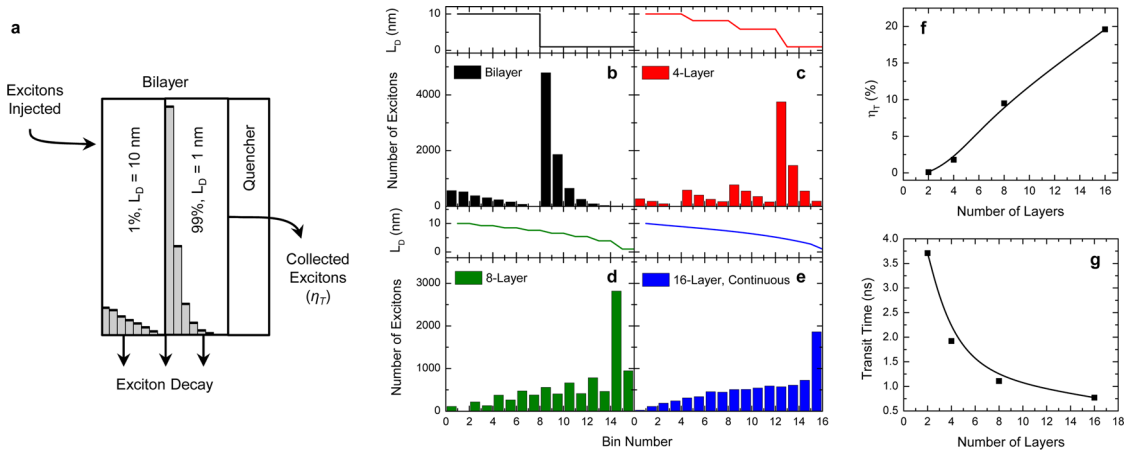

Figure 7. (a) Schematic describing the model experiment to determine the efficiency of exciton transport across these gated systems. (b–e) Histograms representing the recorded locations of exciton decay within the layer as well as the η_T for the various structures. Also shown is the variation in L_D across the layer. (f) Transport efficiency (η_T) as a function of increasing interfaces and defined as the probability that an exciton, injected into the most dilute layer, traverses the entire 16 nm-thick structure. (g) Average transit time for excitons that traverse the entire 16 nm-thick structure and contribute to η_T.

the plot with slopes greater than unity indicate apparent superdiffusive behavior for the overall structure.[47] To verify, Figure 6c displays the derivative of the data in Figure 6b where α, the slope, is defined from $\langle x^2 \rangle = \beta t^{\alpha}$. Values of $\alpha > 1$ and $\alpha < 1$ signify super- and subdiffusive motion, respectively. Clearly, the structures with the greatest number of permeable interfaces show the largest degree of apparent superdiffusive motion, with α reaching a peak value of $\alpha \sim 1.5$. Furthermore, the peak in α occurs at increasingly shorter times as the number of permeable interfaces is increased. We stress that directed energy transfer only occurs at the permeable interface, and energy transfer events within the bulk of a layer still lead to diffusive motion within that given layer.

To investigate how efficiently an exciton can practically traverse the various multilayer structures from Figure 6, excitons are again injected into the most dilute layer. However, now, no injection layer is included, and the excitons are permitted to decay according to their natural lifetime. Excitons that reach the opposite end of the layered system are said to be collected, characterized by a transport efficiency, η_T. The time taken by the excitons to traverse the system is denoted as the transit time. This experiment is depicted schematically in Figure 7a.

A histogram of the final exciton locations for each of the structures is presented in Figure 7b–e. Exciton gating occurs on the more concentrated side of each permeable interface. Additionally, as the number of permeable interfaces increases, the relative difference in exciton density between adjacent bins decreases. This is likely due to smaller imbalances in energy transfer rates across the interface since the changes in concentration occur in finer steps as more interfaces are added. In the 16-layer system, where the rates change continuously, there is a constant increase in exciton density across the structure. Coupled to the deeper penetration of excitons into this system is a concomitant increase in the η_T (Figure 7f). Indeed, nearly 20% of excitons injected into bin 1 are able to traverse the 16 nm layer structure in the 16-layer system even though the average L_D is only ~6 nm. Furthermore, these excitons are collected on a dramatically shorter time scale with the majority being transported below their natural exciton lifetime of $\tau = 1$ ns (Figure 7g). Beyond designing systems for optimal exciton collection, exciton permeable interfaces could also be designed to confine or redistribute excitons faster than could normally be achieved with purely diffusive motion.

From the multiple cases presented in this work, it is clear that exciton permeable interfaces can play an impactful role in engineering exciton transport in planar heterojunction OPVs. In fact, developing an improved understanding of the phenomena that drive imbalances in energy transfer may serve to shift the paradigm from one that simply optimizes diffusion by enhancing L_D or circumvents diffusion *via* the BHJ to one that deeply considers the properties of exciton permeable interfaces.

In the case of the energy-cascade OPVs modeled based on the donor pairing of SubPc and SubNc, variations in the energy-gap are able to increase the η_D for both constituent layers. Such a configuration is favorable in terms of exciton transport since the variation in energy-gap provides the ultimate exciton gate, as energy transfer back to the wider gap donor has a near-zero probability. A similar energetic asymmetry could also be realized using inorganic quantum dots (QDs), where the energy gap is tuned based on QD size *via* quantum confinement. Exciton transport in QD films is also diffusive, or even subdiffusive owing to energetic disorder.[48] To overcome this limit, layered structures with exciton permeable interfaces could be used to introduce a symmetry breaking

imbalance in energy transfer, again achieving directed transport.[49,50]

Energy cascade structures can, however, have an impact on other device parameters, notably the open-circuit-voltage (V_{OC}) due to the resultant change in the molecular orbital energy landscape. Careful selection and alignment of molecular orbital energy levels allows for this limitation to be overcome, with energy-cascade OPVs having shown remarkable η_P.[3] It should be noted that in the case of SubPc and SubNc, significant long-range Förster energy transfer can occur from SubPc to SubNc. While explicitly accounted for the in the simulations presented here, such is not the general case of any donor pairing. Excitons that move *via* the relatively short-range Dexter-type energy transfer will only be able to transfer at the permeable interface, thereby reducing the relative η_D of the outer layer. Since Dexter-type energy transfer is mediated by electron–hole exchange interactions associated with molecular orbital overlap, it stands to reason that diffusion of polarons, which move by a similar mechanism, may also be affected by the incorporation of exciton permeable interfaces. By decoupling the exciton and polaron imbalance across interfaces, their spatial distributions can be separately engineered, offering the ability to design novel devices with an unprecedented level of control over nanoscale transport processes and exciton–polaron interactions.

In dilute donor OPVs that incorporate SubPc in a wide energy gap host material, increases in L_D only describe part of the overall increase in η_D. A significant contribution to the enhanced donor η_D can be attributed to the increasing imbalance in energy transfer from the dilute SubPc layer to the neat SubPc layer with dilution (Figure 4b). Interestingly, the dilute donor OPVs modeled in Figure 2 are reminiscent of the bilayer structures simulated in Figure 6b,c albeit with much different L_D and degree of imbalance. The striking similarity, however, suggests that even larger η_D could be achieved by incorporating multiple interfaces, moving toward the superdiffusive regime expounded by the continuously varying structure with a value of $\alpha \sim 1.5$. Furthermore, collecting excitons at shorter time scales after photogeneration may reduce the steady state exciton density within the layer(s). Such an instance could be advantageous to circumvent exciton–exciton or exciton-charge quenching pathways, leading to further enhancement in the η_D or η_{CC}, respectively.

Beyond dilute donor layers and photovoltaic devices, the notion of superdiffusive exciton transport has the potential to transform a number of other exciton-mediated, optoelectronic devices. The ability to move excitons to a desired location with high fidelity, signaled by α nearing the ballistic limit of $\alpha = 2$, could prove to be an enabling capability for devices such as exciton logic circuits as well as serve to mitigate deleterious exciton–exciton interactions in organic light-emitting devices.

CONCLUSION

Overall, we have detailed the emergent properties of exciton permeable interfaces and their effect on the η_D in highly efficient OPVs. Combined with enhancements in the bulk L_D, the further utilization of exciton permeable interfaces has the ability to fully revitalize interest in the planar heterojunction architecture for next generation OPVs. More broadly, this work demonstrates the utility of exciton permeable interfaces for directing exciton motion, and, in particular, the ability to move excitons quickly—in less than their natural lifetime—to a desired location. The applications for such a toolkit expands beyond OPVs and may be helpful to the broader array of organic optoelectronic devices where excitons play the mediating role in the conversion of light to charge and *vice versa*.

METHODS

Stochastic Simulations. Kinetic Monte Carlo modeling is used to generate simulations for the exciton density profiles η_{EQE}, η_A, and η_D presented in this work. Energy transfer rates for the bulk were derived from a simple, nearest-neighbor interpretation of the exciton diffusivity, $D = L_D^2\tau^{-1} = d^2k$, where d is the discretization of the KMC model, or bin spacing, and k is the energy transfer rate input. Estimates for the molecular densities of each material were obtained from crystallographic information when available and from powder densities otherwise. The exciton generation rate, $Q(x)$, was simulated using transfer matrix formalism of the incident optical field. The optical constants of each material were measured by variable angle spectroscopic ellipsometry. For the simulations of OPV devices, the MoO_x anode buffer layer was approximated as a reflecting boundary.

Device Fabrication. Organic photovoltaic cells were fabricated on glass slides coated with a 150 nm-thick layer of indium–tin–oxide (ITO) having a sheet resistance of 15 Ω/□. All substrates were cleaned with tergitol and solvents. Additionally, ITO substrates were exposed to a UV-ozone ambient for 10 min prior to the deposition of the active layers. Organic layers were deposited *via* vacuum thermal sublimation ($<10^{-7}$ Torr) at a nominal rate of 0.2 nm/s. Devices were capped with a 100 nm-thick cathode layer of Al deposited at a nominal rate of 0.3 nm/s through a shadow mask defining an active area with a diameter of 1 mm. Layer thicknesses were initially optimized *via* transfer matrix simulations of the internal optical field. SubPc, SubNc, and UGH2 were purchased from Luminescence Technology Corporation and C_{60} was purchased from MER Corporation. All materials were used as received with no further purification.

Optoelectronic Characterization. External quantum efficiency testing was performed under illumination from a 300 W xenon lamp coupled to a Cornerstone 130 1/8 m monochromator and chopped with a Stanford Research Systems SR540 optical chopper. Electrical characteristics were measured using a Stanford Research Systems SR810 lock-in amplifier. Devices were also characterized under AM 1.5G solar radiation, and the parameters were extracted from current–voltage testing at an illumination of (100 ± 5) mW/cm^2.

Conflict of Interest: The authors declare no competing financial interest.

Acknowledgment. This work was supported by the National Science Foundation (NSF) under DMR-1006566, DMR-1307066 and CBET-1067681. S.M.M. acknowledges support from a University of Minnesota Doctoral Dissertation Fellowship.

Supporting Information Available: Concentration dependence of interlayer in dilute donor films, details for the artificial dilute donor device simulation, details for the artificial energy cascade device simulation. This material is available free of charge *via* the Internet at http://pubs.acs.org.

REFERENCES AND NOTES

1. Krebs, F. C.; Espinosa, N.; Hösel, M.; Søndergaard, R. R.; Jørgensen, M. 25th Anniversary Article: Rise to Power—OPV-Based Solar Parks. *Adv. Mater.* **2014**, *26*, 29–39.
2. Li, G.; Zhu, R.; Yang, Y. Polymer Solar Cells. *Nat. Photonics* **2012**, *6*, 153–161.
3. Cnops, K.; Rand, B. P.; Cheyns, D.; Verreet, B.; Empl, M. A.; Heremans, P. 8.4% Efficient Fullerene-Free Organic Solar Cells Exploiting Long-Range Exciton Energy Transfer. *Nat. Commun.* **2014**, *5*, 3406.
4. You, J.; Dou, L.; Yoshimura, K.; Kato, T.; Ohya, K.; Moriarty, T.; Emery, K.; Chen, C.; Gao, J.; Li, G.; Yang, Y. A Polymer Tandem Solar Cell with 10.6% Power Conversion Efficiency. *Nat. Commun.* **2013**, *4*, 1446.
5. Xiao, X.; Bergemann, K. J.; Zimmerman, J. D.; Lee, K.; Forrest, S. R. Small-Molecule Planar-Mixed Heterojunction Photovoltaic Cells with Fullerene-Based Electron Filtering Buffers. *Adv. Energy Mater.* **2014**, *4*, 1301557.
6. Wang, D. H.; Kyaw, A. K. K.; Gupta, V.; Bazan, G. C.; Heeger, A. J. Enhanced Efficiency Parameters of Solution-Processable Small-Molecule Solar Cells Depending on ITO Sheet Resistance. *Adv. Energy Mater.* **2013**, *3*, 1161–1165.
7. Meerheim, R.; Körner, C.; Leo, K. Highly Efficient Organic Multi-Junction Solar Cells with a Thiophene Based Donor Material. *Appl. Phys. Lett.* **2014**, *105*, 063306.
8. Zou, Y.; Holst, J.; Zhang, Y.; Holmes, R. J. 7.9% efficient vapor-deposited organic photovoltaic cells based on a simple bulk heterojunction. *J. Mater. Chem.* **2014**, *2*, 12397.
9. Gregg, B. A. Excitonic Solar Cells. *J. Phys. Chem. B* **2003**, *107*, 4688–4698.
10. Menke, S. M.; Holmes, R. J. Exciton Diffusion in Organic Photovoltaic Cells. *Energy Environ. Sci.* **2014**, *7*, 499–512.
11. Menke, S. M.; Luhman, W. A.; Holmes, R. J. Tailored Exciton Diffusion in Organic Photovoltaic Cells for Enhanced Power Conversion Efficiency. *Nat. Mater.* **2013**, *12*, 152–1577.
12. Mullenbach, T. K.; McGarry, K. A.; Luhman, W. A.; Douglas, C. J.; Holmes, R. J. Connecting Molecular Structure and Exciton Diffusion Length in Rubrene Derivatives. *Adv. Mater.* **2013**, *25*, 3689–3693.
13. Mikhnenko, O. V.; Lin, J.; Shu, Y.; Anthony, J. E.; Blom, P. W. M.; Nguyen, T. Q.; Loi, M. A. Effect of Thermal Annealing on Exciton Diffusion in a Diketopyrrolopyrrole Derivative. *Phys. Chem. Chem. Phys.* **2012**, *14*, 14196.
14. Masri, Z.; Ruseckas, A.; Emelianova, E. V.; Wang, L.; Bansal, A. K.; Matheson, A.; Lemke, H. T.; Nielsen, M. M.; Nguyen, H.; Coulembier, O.; Dubois, P.; Beljonne, D.; Samuel, I. D. W. Molecular Weight Dependence of Exciton Diffusion in Poly(3-hexylthiophene). *Adv. Energy Mater.* **2013**, *3*, 1445–1453.
15. Fennel, F.; Lochbrunner, S. Long Distance Energy Transfer in a Polymer Matrix Doped with a Perylene Dye. *Phys. Chem. Chem. Phys.* **2011**, *13*, 3527–3533.
16. Lunt, R. R.; Benziger, J. B.; Forrest, S. R. Relationship between Crystalline Order and Exciton Diffusion Length in Molecular Organic Semiconductors. *Adv. Mater.* **2010**, *22*, 1233.
17. Najafov, H.; Lee, B.; Zhou, Q.; Feldman, L. C.; Podzorov, V. Observation of Long-Range Exciton Diffusion in Highly Ordered Organic Semiconductors. *Nat. Mater.* **2010**, *9*, 938–943.
18. Luhman, W. A.; Holmes, R. J. Enhanced Exciton Diffusion in an Organic Photovoltaic Cell by Energy Transfer using a Phosphorescent Sensitizer. *Appl. Phys. Lett.* **2009**, *94*, 153304.
19. Rand, B. P.; Schols, S.; Cheyns, D.; Gommans, H.; Girotto, C.; Genoe, J.; Heremans, P.; Poortmans, J. Organic Solar Cells with Sensitized Phosphorescent Absorbing Layers. *Org. Electron.* **2009**, *10*, 1015–1019.
20. Markov, D. E.; Tanase, C.; Blom, P. W. M.; Wildeman, J. Simultaneous Enhancement of Charge Transport and Exciton Diffusion in Poly(p-Phenylene Vinylene) Derivatives. *Phys. Rev. B* **2005**, *72*, 045217.
21. Halls, J. J. M.; Walsh, C. A.; Greenham, N. C.; Marseglia, E. A.; Friend, R. H.; Moratti, S. C.; Holmes, A. B. Efficient Photodiodes from Interpenetrating Polymer Networks. *Nature* **1995**, *376*, 498–500.
22. Yu, G.; Gao, J.; Hummelen, J. C.; Wudl, F.; Heeger, A. J. Polymer Photovoltaic Cells: Enhanced Efficiencies *via* a Network of Internal Donor-Acceptor Heterojunctions. *Science* **1995**, *270*, 1789–1791.
23. Nelson, J. Polymer: Fullerene Bulk Heterojunction Solar Cells. *Mater. Today* **2011**, *14*, 462–470.
24. Ashcroft, N. W.; Mermin, N. D. *Solid State Physics*; Saunders College: Belmont, CA, 1976; p 826.
25. Hagn, M.; Zrenner, A.; Böhm, G.; Weimann, G. Electric-field-induced Exciton Transport in Coupled Quantum Well Structures. *Appl. Phys. Lett.* **1995**, *67*, 232–234.
26. High, A. A.; Hammack, A. T.; Butov, L. V.; Hanson, M.; Gossard, A. C. Exciton Optoelectronic Transistor. *Opt. Lett.* **2007**, *32*, 2466–2468.
27. High, A. A.; Novitskaya, E. E.; Butov, L. V.; Hanson, M.; Gossard, A. C. Control of Exciton Fluxes in an Excitonic Integrated Circuit. *Science* **2008**, *321*, 229–231.
28. Berggren, M.; Dodabalapur, A.; Slusher, R. E.; Bao, Z. Light Amplification in Organic Thin Films Using Cascade Energy Transfer. *Nature* **1997**, *389*, 466–469.
29. Kim, J.; McQuade, D. T.; Rose, A.; Zhu, Z.; Swager, T. M. Directing Energy Transfer within Conjugated Polymer Thin Films. *J. Am. Chem. Soc.* **2001**, *123*, 11488–11489.
30. Ameri, T.; Khoram, P.; Min, J.; Brabec, C. J. Organic Ternary Solar Cells: A Review. *Adv. Mater.* **2013**, *25*, 4245–4266.
31. Schlenker, C. W.; Barlier, V. S.; Chin, S. W.; Whited, M. T.; McAnally, R. E.; Forrest, S. R.; Thompson, M. E. Cascade Organic Solar Cells. *Chem. Mater.* **2011**, *23*, 4132–4140.
32. Barito, A.; Sykes, M. E.; Huang, B.; Bilby, D.; Frieberg, B.; Kim, J.; Green, P. F.; Shtein, M. Universal Design Principles for Cascade Heterojunction Solar Cells with High Fill Factors and Internal Quantum Efficiencies Approaching 100%. *Adv. Energy Mater.* **2014**, *4*, 1400216.
33. Grob, S.; Gruber, M.; Bartynski, A. N.; Hörmann, U.; Linderl, T.; Thompson, M. E.; Brütting, W. Amorphous *vs* Crystalline Exciton Blocking Layers at the Anode Interface in Planar and Planar-Mixed Heterojunction Organic Solar Cells. *Appl. Phys. Lett.* **2014**, *104*, 213304.
34. Menke, S. M.; Holmes, R. J. Energy-Cascade Organic Photovoltaic Devices Incorporating a Host−Guest Architecture. *ACS Appl. Mater. Interfaces* **2015**, *7*, 2912–2918.
35. Pettersson, L. A. A.; Roman, L. S.; Inganas, O. Modeling Photocurrent Action Spectra of Photovoltaic Devices Based on Organic Thin Films. *J. Appl. Phys.* **1999**, *86*, 487–496.
36. Gommans, H.; Cheyns, D.; Aernouts, T.; Girotto, C.; Poortmans, J.; Heremans, P. Electro-Optical Study of Subphthalocyanine in a Bilayer Organic Solar Cell. *Adv. Funct. Mater.* **2007**, *17*, 2653–2658.
37. Gommans, H.; Schols, S.; Kadashchuk, A.; Heremans, P.; Meskers, S. C. J. Exciton Diffusion Length and Lifetime in Subphthalocyanine Films. *J. Phys. Chem. C* **2009**, *113*, 2974–2979.
38. Morse, G. E.; Bender, T. P. Boron Subphthalocyanines as Organic Electronic Materials. *ACS Appl. Mater. Interfaces* **2012**, *4*, 5055–5068.
39. Holmes, R. J.; D'Andrade, B. W.; Forrest, S. R.; Ren, X.; Li, J.; Thompson, M. E. Efficient, Deep-Blue Organic Electrophosphorescence by Guest Charge Trapping. *Appl. Phys. Lett.* **2003**, *83*, 3818–3820.

40. Zou, Y.; Holmes, R. J. Influence of a MoOx Interlayer on the Open-Circuit Voltage in Organic Photovoltaic Cells. *Appl. Phys. Lett.* **2013**, *103*, 053302.
41. Coffey, D. C.; Ferguson, A. J.; Kopidakis, N. Rumbles, G. Photovoltaic Charge Generation in Organic Semiconductors Based on Long-Range Energy Transfer. *ACS Nano* **2010**, *4*, 5437–5445.
42. Scully, S. R.; Armstrong, P. B.; Edder, C.; Fréchet, J. M. J.; McGehee, M. D. Long-Range Resonant Energy Transfer for Enhanced Exciton Harvesting for Organic Solar Cells. *Adv. Mater.* **2007**, *19*, 2961.
43. Verreet, B.; Cnops, K.; Cheyns, D.; Heremans, P.; Stesmans, A.; Zango, G.; Claessens, C. G.; Torres, T.; Rand, B. P. Decreased Recombination through the Use of a Non-Fullerene Acceptor in a 6.4% Efficient Organic Planar Heterojunction Solar Cell. *Adv. Energy Mater.* **2014**, *4*, No. 1301413.
44. Ma, B.; Woo, C. H.; Miyamoto, Y.; Fréchet, J. M. J. Solution Processing of a Small Molecule, Subnaphthalocyanine, for Efficient Organic Photovoltaic Cells. *Chem. Mater.* **2009**, *21*, 1413–1417.
45. Förster, T. 10th Spiers Memorial Lecture. Transfer Mechanisms of Electronic Excitation. *Discuss. Faraday Soc.* **1959**, *27*, 7.
46. Luhman, W. A.; Holmes, R. J. Investigation of Energy Transfer in Organic Photovoltaic Cells and Impact on Exciton Diffusion Length Measurements. *Adv. Funct. Mater.* **2011**, *21*, 764–771.
47. Akselrod, G. M.; Deotare, P. B.; Thompson, N. J.; Lee, J.; Tisdale, W. A.; Baldo, M. A.; Menon, V. M.; Bulović, V. Visualization of Exciton Transport in Ordered and Disordered Molecular Solids. *Nat. Commun.* **2014**, *5*, No. 3646.
48. Akselrod, G. M.; Prins, F.; Poulikakos, L. V.; Lee, E. M. Y.; Weidman, M. C.; Mork, A. J.; Willard, A. P.; Bulović, V.; Tisdale, W. A. Subdiffusive Exciton Transport in Quantum Dot Solids. *Nano Lett.* **2014**, *14*, 3556–3562.
49. Klar, T. A.; Franzl, T.; Rogach, A. L.; Feldmann, J. Super-Efficient Exciton Funneling in Layer-by-Layer Semiconductor Nanocrystal Structures. *Adv. Mater.* **2005**, *17*, 769–773.
50. Ruland, A.; Schulz-Drost, C.; Sgobba, V.; Guldi, D. M. Enhancing Photocurrent Efficiencies by Resonance Energy Transfer in CdTe Quantum Dot Multilayers: Towards Rainbow Solar Cells. *Adv. Mater.* **2011**, *23*, 4573–4577.